OUKA
The University of Osaka
Institutional Knowledge Archive

Title	Oxygen-vacancy defect in 4H-SiC as a near-infrared emitter: An ab initio study
Author(s)	Kobayashi, Takuma; Shimura, Takayoshi; Watanabe, Heiji
Citation	Journal of Applied Physics. 2023, 134(14), p. 145701
Version Type	VoR
URL	https://hdl.handle.net/11094/106891
rights	This article may be downloaded for personal use only. Any other use requires prior permission of the author and AIP Publishing. This article appeared in (J. Appl. Phys. 134, 145701 (2023) and may be found at https://doi.org/10.1063/5.0169147.
Note	

The University of Osaka Institutional Knowledge Archive : OUKA

https://ir.library.osaka-u.ac.jp/

The University of Osaka

Journal of Applied Physics

RESEARCH ARTICLE | OCTOBER 11 2023

Oxygen-vacancy defect in 4H-SiC as a near-infrared emitter: An *ab initio* study

Takuma Kobayashi ; Takayoshi Shimura ; Heiji Watanabe

Check for updates

J. Appl. Phys. 134, 145701 (2023)
https://doi.org/10.1063/5.0169147

View Online Export Citation

Articles You May Be Interested In

A first-principles investigation of halogen doped diamond and its application to quantum technologies

J. Appl. Phys. (September 2025)

The effect of ions on the magnetic moment of vacancy for ion-implanted 4H-SiC

J. Appl. Phys. (April 2017)

Design of annealing conditions for the formation of isolated single-photon emitters at SiO_2/SiC interfaces

J. Appl. Phys. (May 2025)

23 October 2026 02:01:49

Nanotechnology & Materials Science
Optics & Photonics
Impedance Analysis
Scanning Probe Microscopy
Sensors
Failure Analysis & Semiconductors

Unlock the Full Spectrum.
From DC to 8.5 GHz.



Zurich Instruments

Find out more

AIP Publishing

Journal of Applied Physics ARTICLE pubs.aip.org/aip/jap

Oxygen-vacancy defect in 4H-SiC as a near-infrared emitter: An *ab initio* study

Cite as: J. Appl. Phys. **134**, 145701 (2023); doi: 10.1063/5.0169147
Submitted: 23 July 2023 · Accepted: 25 September 2023 ·
Published Online: 11 October 2023

View Online Export Citation CrossMark

Takuma Kobayashi,[a] Takayoshi Shimura, and Heiji Watanabe

AFFILIATIONS

Graduate School of Engineering, Osaka University, Suita, Osaka 565-0871, Japan

[a]**Author to whom correspondence should be addressed:** kobayashi@prec.eng.osaka-u.ac.jp

ABSTRACT

Optically active spin defects in semiconductors can serve as spin-to-photon interfaces, key components in quantum technologies. Silicon carbide (SiC) is a promising host of spin defects thanks to its wide bandgap and well-established crystal growth and device technologies. In this study, we investigated the oxygen-vacancy complexes as potential spin defects in SiC by means of *ab initio* calculations. We found that the O_CV_{Si} defect has a substantially low formation energy compared with its counterpart, $O_{Si}V_C$, regardless of the Fermi level position. The O_CV_{Si} defect is stable in its neutral charge state with a high-spin ground state ($S = 1$) within a wide energy range near the midgap energy. The zero-phonon line (ZPL) of the $O_CV_{Si}^0$ defect lies in the near-infrared regime, 1.11–1.24 eV (1004–1117 nm). The radiative lifetime for the ZPL transition of the defect in kk configuration is fairly short (12.5 ns). Furthermore, the estimated Debye–Waller factor for the optical transition is 13.4%, indicating a large weight of ZPL in the photoluminescence spectrum. All together, we conclude that the $O_CV_{Si}^0$ defect possesses desirable spin and optical properties and thus is potentially attractive as a quantum bit.

Published under an exclusive license by AIP Publishing. https://doi.org/10.1063/5.0169147

23 October 2026 02:01:49

I. INTRODUCTION

Spin defects in semiconductors are leading candidates for quantum bits, which are a fundamental building block in quantum applications including quantum computing[1] and quantum cryptography.[2] Furthermore, if the defect is optically addressable, it may serve as a spin-to-photon interface.[2,3] Diamond is a wide bandgap material that hosts many attractive spin defects. The negatively charged nitrogen–vacancy (NV) center is a leading example, featuring a long spin coherence time and bright luminescence even at room temperature.[4,5] In addition to the experimentally identified group-IV complexes such as silicon–vacancy (SiV)[6] and germanium–vacancy (GeV)[7] centers, oxygen-related defects have also been studied in detail at an *ab initio* level.[8,9] In particular, the neutral oxygen–vacancy (OV) defect seemed promising at first glance because it is isovalent to the negatively charged NV center. Nevertheless, it turned out that the lowest energy excited state of this defect comprises C–O antibonding orbitals, leading to a fast nonradiative decay from the optical excited state to the ground state.[8]

Silicon carbide (SiC) is a wide-bandgap semiconductor that shares favorable material properties with diamond.[10–12] Furthermore, the defect spins in SiC can have longer coherence times than in diamond, because of the suppressed heteronuclear-spin flip–flop process[13] and decoupling of the ^{29}Si and ^{13}C nuclear spin bath[14] in the presence of a magnetic field and the diluted homo-nuclear spin pairs.[14] In addition, well-established crystal growth, doping control, and device technologies make this material striking as a potential host for spin defects.[10] A number of spin defects have indeed been reported so far in SiC. For instance, the negatively charged silicon vacancy (V_{Si}) is a spin-3/2 defect which has zero-phonon lines (ZPL) at 861–917 nm.[15–17] Despite the lack of crystal inversion symmetry, the identical ground and excited states of this defect make its optical transition less sensitive to stray electric fields.[18] The neutral divacancy ($V_{Si}V_C$) is a spin-1 defect with ZPL at 1078–1132 nm.[19,20] Suppressed spin-mixing in the excited state of this defect enables efficient optical readout of electron spins.[21] To exploit the full potential of SiC as a quantum material, further exploration of optically active point defects with non-zero spins will be required.

Motivated by the prior studies in diamond,[8,9] we investigated the oxygen–vacancy complexes in 4H-polytype of SiC (4H-SiC) by means of *ab initio* calculations in this study. Although these defects have been argued to be the emitters found at the SiO_2/SiC interface,[22,23] their potential as a bulk defect has not been clarified yet. We show that the O_CV_{Si} defects possess desirable spin and optical

Published under an exclusive license by AIP Publishing

properties and thus would be prominent candidates for optically addressable spin qubits in SiC.

II. CALCULATION METHODS

A. Computational details

Calculations were performed within the framework of density functional theory,[24,25] using the projector augmented-wave method[26] as implemented in Vienna *ab initio* simulation package (VASP).[27,28] The plane wave cutoff energies in the calculations were set to 550 and 400 eV for perfect 4H-SiC and defect systems, respectively. The Heyd–Scuseria–Ernzerhof (HSE06) hybrid functional[29,30] was used in most of the calculations except those of the zero-field splitting (ZFS) and vibronic modes, where the Perdew–Burke–Ernzerhof (PBE) functional[31] was used instead. VASPKIT[32] and VESTA[33] were used to visualize the spin density and wavefunctions.

B. Modeling of defects

The atom positions and lattice constants of perfect 4H-SiC were optimized using the 8-atom primitive cell with $8\times8\times2$ k-point sampling. The resulting lattice constants are 3.07 and 10.05 Å for the crystal a and c axes, respectively, and are close to the experimental values of 3.08 and 10.08 Å.[10] The defect formation energy and charge transition levels were calculated using a 400-atom $(5\times5\times2)$ supercell with Γ-point-only sampling. During the structural optimization of the defect systems, the lattice constants were kept fixed to the values above, while the positions of the atoms were relaxed so that the Hellman–Feynman forces acting on them would become less than 40 meV Å^{-1}. The formation energy $E_{\rm form}$ of a defect D in the charge state q is calculated as

$$E_{\rm form}[{\rm D}^q] = (E[{\rm D}^q] + E_c[{\rm D}^q]) - E_p - \sum_i n_i\mu_i + q(\varepsilon_{\rm VBM} + \Delta\varepsilon_{\rm F}), \tag{1}$$

where $E[{\rm D}^q]$ and $E_{\rm p}$ are the total energies of the defect system and perfect 4H-SiC supercell, respectively. $E_{\rm C}[{\rm D}^q]$ is a charge correction term, wherein we applied a monopole correction scheme.[34] n_i and μ_i are the number of added ($n_i>0$) or removed ($n_i<0$) i-type atomic species and their chemical potential, respectively. In particular, we assumed that the chemical potential of oxygen atoms equals half of the energy of the oxygen molecule in its triplet state ($\mu_{\rm O}=-7.0$ eV). The sum of the chemical potentials of silicon and carbon atoms equals the total energy of SiC per formula unit ($\mu_{\rm Si}+\mu_{\rm C}=-17.5$ eV). Note that there was no need to determine $\mu_{\rm Si}$ and $\mu_{\rm C}$ independently, because equal numbers of Si and C atoms were removed from the supercell to produce the defects investigated in this study. $\varepsilon_{\rm VBM}$ is the energy of the valence band maximum (VBM) and $\Delta\varepsilon_{\rm F}$ is the Fermi level with respect to $\varepsilon_{\rm VBM}$. Usage of the HSE06 functional is crucial to obtaining proper charge transition levels and wavefunctions, because it satisfies the generalized Koopman's theorem[35,36] for point defects in group-IV materials including diamond, Si, and Ge.[37] A systematic investigation of native point defects in 4H-SiC was previously carried out using the HSE06 functional.[38] After determining the stable defect configurations, we focused on neutral O_CV_{Si} defects and investigated their spin and optical properties by using the optimized structures on larger supercells. Most of the quantities were obtained using a 576-atom $(6\times6\times2)$ supercell, while the transition dipole moment (TDM) was calculated using a 784-atom $(7\times7\times2)$ supercell. Here, the force conversion criterion and k-point sampling condition were the same as above. In the 576-atom perfect 4H-SiC supercell, the conduction band minimum (M-point) folded onto the Γ-point. The resulting bandgap, 3.17 eV, is consistent with the experimental value of 3.26 eV at room temperature.[10]

C. Spin properties

The zero-field splitting (ZFS)[39] and the hyperfine coupling constants[40] were calculated as implemented in VASP. Considering the electron spin dipole–dipole interaction, the zero-field splitting tensor D_{ij} can be written as

$$D_{ij} = \frac{1}{2S(2S-1)}\frac{\mu_0 g_e^2\mu_B^2}{4\pi}\sum_{m<n}\chi_{mn}\int|\Psi_{mn}(\boldsymbol{r}_1,\boldsymbol{r}_2)|^2\left(\frac{r^2\delta_{ij}-3r_ir_j}{r^5}\right)d\boldsymbol{r}_1 d\boldsymbol{r}_2, \tag{2}$$

where S, μ_0, g_e, and μ_B are the total spin, the vacuum magnetic permeability, the Landé g-factor of free electrons, and the Bohr magneton, respectively. χ_{mn} is +1 (−1) for the parallel (anti-parallel) spins. The two-particle wavefunction $\Psi_{mn}(\boldsymbol{r}_1,\boldsymbol{r}_2)$ can be approximated as the Slater determinant of the Kohn–Sham orbitals ψ_m and ψ_n.[39] r and r_i, respectively, denote the absolute value and components of the vector $\boldsymbol{r}_1-\boldsymbol{r}_2$. The axial and transversal components of the ZFS parameters D and E were derived from the principal values D_{xx}, D_{yy}, and D_{zz} as follows:

$$D = \frac{3}{2}D_{zz},\ E = \frac{D_{yy}-D_{xx}}{2}. \tag{3}$$

The D and E parameters were calculated from the pseudowavefunctions computed by VASP without applying PAW core corrections. The PBE functional was used, as it gives values that are consistent with experiment for point defects in diamond and SiC.[39,41] The hyperfine tensor A_{ij} describing the interaction between the electron spin and nuclear spin is given as

$$A_{ij} = \frac{\mu_0 g_e\mu_B g_N\mu_N}{4\pi S}\int\rho_s(\boldsymbol{r})\left(\frac{8\pi}{3}\delta(r)+\frac{3r_ir_j-r^2\delta_{ij}}{r^5}\right)d\boldsymbol{r}, \tag{4}$$

where g_N, μ_N, and $\rho_s(\boldsymbol{r})$ are the Landé g-factor of nuclear, nuclear magneton, and electron spin density, respectively. The first and second terms in the brackets represent the Fermi-contact and magnetic dipole–dipole interaction terms, respectively. We used the HSE06 functional in the calculation of the hyperfine constants. The contribution of the core electrons to the Fermi contact term was taken into account under the frozen valence approximation.[42]

23 October 2026 02:01:49

Published under an exclusive license by AIP Publishing

D. Optical properties

The excited state of a defect was studied within the constrained occupation method (ΔSCF method), which was first applied to the diamond NV center by Gali *et al.*[43] The calculated ZPL values of the diamond NV center,[43,44] and V_{Si}[45] and $V_{Si}V_C$[46] in SiC agree well with experiment within an error of about 0.1 eV. The radiative lifetime of the excited state is calculated from the TDM vector. The TDM vector $\boldsymbol{\mu}$ is calculated by

$$\boldsymbol{\mu} = \frac{i\hbar}{(\varepsilon_f - \varepsilon_i)m_e}\left\langle \psi_f | \boldsymbol{p} | \psi_i \right\rangle, \tag{5}$$

where ψ_f and ψ_i are the orbitals of final and initial states, ε_f and ε_i are their eigenvalues, and m_e is the electron mass. The ground- and excited-state wavefunctions computed by VASP were post-processed with PyVaspwfc[47] in order to calculate the TDM vector. In this study, the code was modified so that it could handle two wavefunctions instead of one, as described in Ref. 48. This enables the radiative lifetime of the ZPL transition to be calculated. The radiative lifetime τ_{rad} can then be calculated from the Einstein coefficient A as

$$\tau_{rad} = \frac{1}{A} = \frac{3\pi\epsilon_0\hbar c^3}{n\omega^3|\boldsymbol{\mu}|^2}. \tag{6}$$

Here, ϵ_0, c, ω, and n are the vacuum permittivity, the speed of light, the transition frequency of ZPL, and the refractive index of 4H-SiC ($n = 2.6473$), respectively.

The photoluminescence (PL) line shape was calculated within the Huang–Rhys theory by using a generating function approach.[49] Here, the normalized PL intensity $I(\hbar\omega)$ with a photon energy of $\hbar\omega$ is expressed in the form

$$I(\hbar\omega) = \omega^3 A(\hbar\omega), \tag{7}$$

where $A(\hbar\omega)$ is the optical spectral function,

$$A(\hbar\omega) = \frac{1}{2\pi}\int_{-\infty}^{+\infty} G(t)e^{i\omega t - \gamma|t|}dt. \tag{8}$$

$G(t)$ is the generating function, defined as

$$G(t) = e^{S(t) - S(0)}, \tag{9}$$

where

$$S(t) = \int_0^{+\infty} S(\hbar\omega)e^{-i\omega t}d(\hbar\omega), \tag{10}$$

and

$$S(\hbar\omega) = \sum_i S_i\delta(\hbar\omega - \hbar\omega_i). \tag{11}$$

$S(\hbar\omega)$, S_i, and ω_i are the spectral function of electron–phonon coupling, the partial Huang–Rhys factor for the ith phonon mode, and the frequency of the ith phonon, respectively. In this study, the broadening of ZPL γ in Eq. (8) was set to a certain value and is not a derived quantity. The δ functions in Eq. (11) were replaced by 6-meV-wide Gaussians. The total Huang–Rhys factor S and the Debye–Waller factor W were derived as

$$S = \sum_i S_i \text{ and } W = e^{-S}. \tag{12}$$

In the calculation of the defect-perturbed vibronic modes, the structures with displacements were prepared by phonopy, sets of forces were calculated by VASP, and the forces were post-processed by phonopy[50] under the harmonic approximation. Then, the VASP and phonopy outputs were post-processed by PyPhotonics software[51] in order to compute the PL line shape. Here, while the structures of the ground and excited states were optimized with the HSE06 functional, the vibronic modes were calculated at a PBE level. Such an approach saves computational time while maintaining sufficient accuracy.[44,52]

III. RESULTS AND DISCUSSION

A. Structure and formation energies of oxygen-vacancy defects

Figure 1 shows the formation energy of OV defects in 4H-SiC, while Fig. 2 shows the structure of the defects in the kk configuration. As can be seen in Fig. 1, the O_CV_{Si} defects are the most stable regardless of the position of the Fermi level. For the kk and hh configurations, the O atom lies on the symmetry axis of the crystal, realizing C_{3v} symmetry (Fig. 2). Note that the three carbon atoms with dangling bonds are relaxed outward from the vacant site and do not form long bonds with each other. We confirmed that even when the structural optimization is started from a low-symmetry

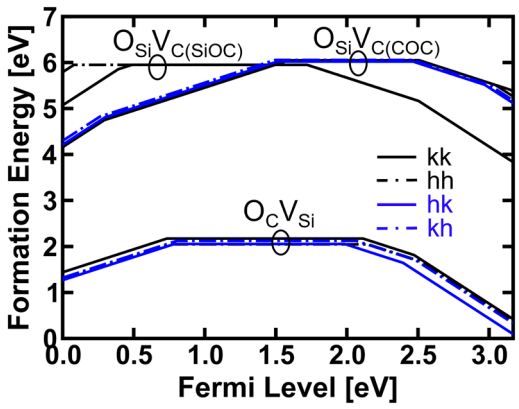


FIG. 1. Formation energy as a function of the Fermi level for OV defect complexes in 4H-SiC calculated using the HSE06 functional. The results for three different types of stable (meta-stable) defect are shown; i.e., O_CV_{Si}, $O_{Si}V_{C(COC)}$, and $O_{Si}V_{C(SiOC)}$. The zero of the Fermi level corresponds to the valence band maximum, while the conduction band minimum is located at the right end of the figure (i.e., 3.17 eV). The structure of each defect in its kk configuration is shown in Fig. 2.

23 October 2026 02:01:49

Published under an exclusive license by AIP Publishing

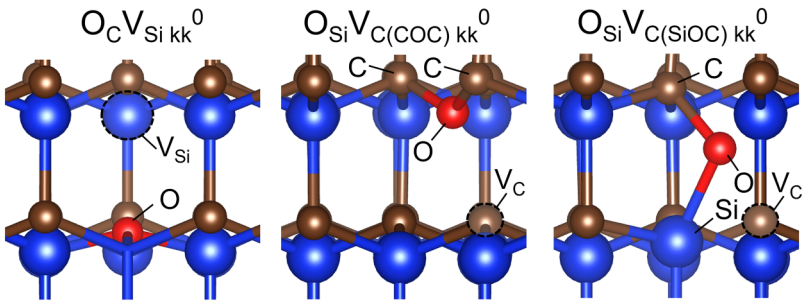


FIG. 2. Optimized structures of neutral OV defect complexes in 4H-SiC. The results for the kk configuration are depicted and the structures are viewed perpendicular to the crystal c axis. Blue, brown, and red spheres represent Si, C, and O atoms, respectively.

geometry, a high-symmetry structure is eventually obtained. The resulting length of the Si–O bonds is 1.83 Å, short compared with the C–Si bonds in a perfect SiC crystal (1.88 Å), and the Si–O–Si bond angle is 116°. For the hk and kh configurations, the O atom is threefold coordinated and the carbon dangling bonds are strongly localized in a similar manner, but the symmetry is lowered to C_{1h} due to the off-axis configurations.

For the $O_{Si}V_C$ complex, we find two different types of defect having similar formation energies in the neutral charge state; i.e., $O_{Si}V_{C(COC)}$ and $O_{Si}V_{C(SiOC)}$. The O atom is bonded to two C atoms in the former, while it is bonded to one Si atom and one C atom in the latter (Fig. 2). Under the p-type (n-type) condition, the $O_{Si}V_{C(COC)}$ defects are more (less) stable than the $O_{Si}V_{C(SiOC)}$ defects. For the $O_{Si}V_{C(COC)}$ defects, the length of the C–O bonds and the bond angle of C–O–C are 1.52 Å and 116°, respectively. While the $O_{Si}V_{C(COC)}$ defects are stabilized in all the kk, hh, hk, and kh configurations, the $O_{Si}V_{C(SiOC)}$ defects are only stabilized in the kk and hh configurations. This is because the minimum distance between the Si and C atoms that the O atom has to connect to is longer (3.60 Å) in the hk and kh complexes than in the kk and hh ones (3.14 Å) before the relaxation takes place. Regarding the $O_{Si}V_{C(SiOC)}$ defects, the lengths of the Si–O bond and C–O bond are 1.86 and 1.49 Å, respectively, and the bond angle of Si–O–C is 108°. Table I summarizes the formation energies of the neutral OV defects. Regardless of the configuration (kk, hh, hk, or kh), the O_CV_{Si} defects have substantially lower formation energy compared with the other investigated OV defects.

The charge transition levels of the O_CV_{Si} defect are summarized in Table II. We find that the O_CV_{Si} defects take a charge state from +1 to −2 depending on the Fermi level position. However, it can be seen that the neutral charge state is favorable within a wide energy range near the midgap energy (from about $\varepsilon_{VBM} + 0.7$ eV to $\varepsilon_{VBM} + 2.2$ eV). We thus switched to using larger supercells (576- or 784-atom) and investigated the spin and optical properties of neutral O_CV_{Si} defects (see Secs. III B and III C).

TABLE I. Formation energies of neutral OV defects in 4H-SiC obtained using the HSE06 functional (unit: eV). Typical structures of defects in the kk configuration are shown in Fig. 2.

	Formation energies
$O_CV_{Si\ kk}^0$	2.17
$O_CV_{Si\ hh}^0$	2.05
$O_CV_{Si\ hk}^0$	2.05
$O_CV_{Si\ kh}^0$	2.12
$O_{Si}V_{C(COC)\ kk}^0$	6.05
$O_{Si}V_{C(COC)\ hh}^0$	6.05
$O_{Si}V_{C(COC)\ hk}^0$	6.02
$O_{Si}V_{C(COC)\ kh}^0$	6.06
$O_{Si}V_{C(SiOC)\ kk}^0$	5.95
$O_{Si}V_{C(SiOC)\ hh}^0$	5.95

B. Spin properties of the $O_CV_{Si}^0$ defects

Figure 3 shows the single-particle energy diagrams for the $O_CV_{Si}^0$ defects. We find that the $O_CV_{Si}^0$ defects exhibit a high-spin ground state ($S = 1$) regardless of the configuration (kk, hh, hk, or kh). For every defect complex, the in-gap states are fully occupied with electrons in the spin majority channel. In contrast, only some of the states are occupied in the spin minority channel. For the hh and kk complexes, the empty states are doubly degenerate e states according to the C_{3v} symmetry. In contrast, for the hk and kh complexes, the e states split into a′ and a″ states due to the symmetry being lowered to C_{1h}. The energy differences between the highest occupied orbital and the lowest unoccupied orbital are 1.75, 1.80, 1.61, and 1.73 eV for the kk, hh, hk, and kh complexes, respectively. However, as described in Sec. III C, these energy differences in the Kohn–Sham orbitals overestimate the energies of the optical transition between those states mainly because of the electron–hole coupling.

Figure 4 visualizes the Kohn–Sham wavefunctions corresponding to the single-particle states a_1 and e of the kk complex. The a_1 state is fully symmetric, and the e states consist of carbon dangling bond orbitals. They are the only in-gap states found in the energy

TABLE II. Charge transition levels of O_CV_{Si} defects in 4H-SiC obtained using the HSE06 functional. The energies are with respect to the energy of the valence band maximum (unit: eV).

	(+1/0)	(0/−1)	(−1/−2)
$O_CV_{Si\ kk}$	0.73	2.11	2.47
$O_CV_{Si\ hh}$	0.76	2.15	2.52
$O_CV_{Si\ hk}$	0.79	1.98	2.40
$O_CV_{Si\ kh}$	0.80	2.06	2.48

23 October 2026 02:01:49

Published under an exclusive license by AIP Publishing

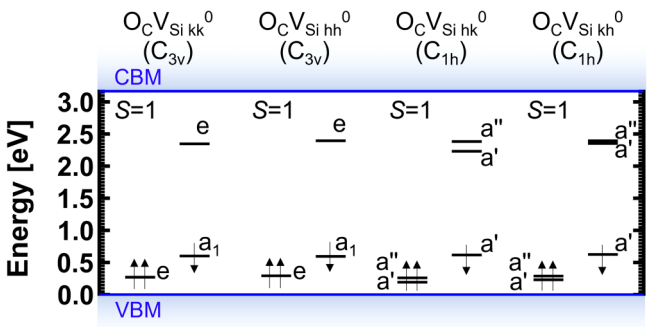


FIG. 3. Single-particle energy levels of $O_CV_{Si}^0$ defects in 4H-SiC calculated using the HSE06 functional. Only in-gap levels are depicted. All the defects are in the high-spin ground state ($S = 1$). While the kk and hh configurations possess C_{3v} symmetry, the symmetry is lowered to C_{1h} for the hk and kh configurations. The occupancy of the spin minority and minority channels are separately shown for each defect.

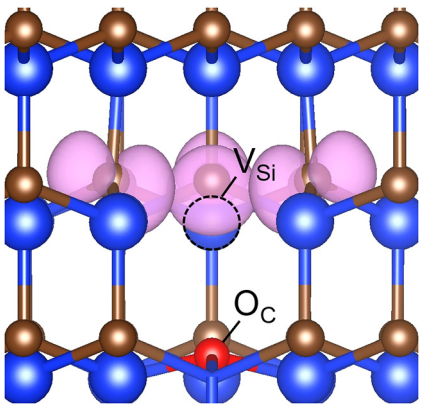


FIG. 5. Spin density of $O_CV_{Si}^0$ defect in the kk configuration in 4H-SiC viewed perpendicular to the c axis. The isosurface of 10% of the maximum amplitude is depicted. The color code of atoms is the same as in Fig. 2, while the spin density is depicted as a pink lobe.

gap (Fig. 3), closely resembling the electronic structure of the diamond NV center. Most importantly, the anti-bonding orbitals of the Si–O bonds are resonant with the conduction band and do not appear within the bandgap in the case of SiC. This is the crucial difference from the case of OV centers in diamond, where the lowest unoccupied energy state consists of the C–O anti-bonding orbitals.[8] This is why the excited state of diamond OV centers is unstable, leading to fast non-radiative decay to the ground state. Since this is not an issue with SiC $O_CV_{Si}^0$ defects, we can expect that the luminescence from them will be stable (see Sec. III C).

Figure 5 shows the calculated spin density of the ground-state $O_CV_{Si}^0$ defect in the kk configuration. The spin is mostly found at the carbon dangling bonds like in the diamond NV center.[53] The calculated ZFS parameters of the $O_CV_{Si}^0$ defects are shown in Table III. The axial component D is in the range of 1.61–1.74 GHz depending on the configuration. The sign of D indicates that the $m_S = \pm 1$ sublevels are located above the $m_S = 0$ sublevel in the absence of an external magnetic field. The transversal component E vanishes for the kk and hh configurations because of the symmetry, but shows finite values of 0.15 and 0.04 GHz for the lower-symmetry hk and kh configurations, respectively.

We also calculated the principal values of the hyperfine tensor for the $O_CV_{Si}^0$ defects, which could be used to identify the defects as well as the coupling of the defect spins with nearby nuclear spins. The calculated principal values are summarized in Table IV. As expected from the spin density being mostly localized at the carbon dangling bonds (Fig. 5), the largest hyperfine interactions are found at the three C atoms adjacent to the vacant site when they contain a ^{13}C isotope with an $I = 1/2$ nuclear spin. Principal values of around 7–14 MHz are also found at the nine Si atoms connected to the three C atoms with dangling bonds, when they are the ^{29}Si isotope with $I = 1/2$ nuclear spin. The O atoms indicate hyperfine constant of 2–5 MHz when they contain ^{17}O isotope with an $I = 5/2$ nuclear spin. Although the natural abundance of

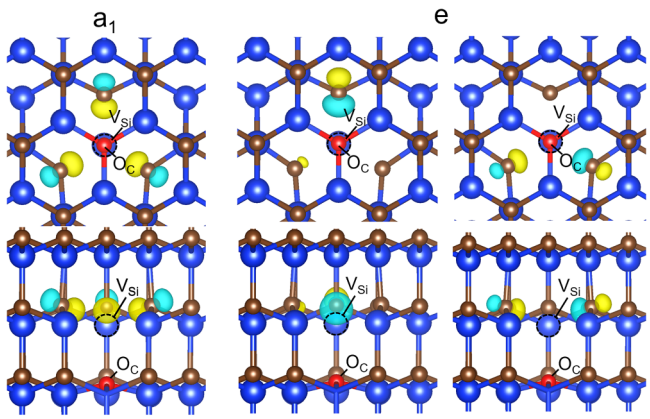


FIG. 4. Kohn–Sham orbitals of the $O_CV_{Si}^0$ defect in the kk configuration in 4H-SiC obtained using the HSE06 functional. The structures are viewed along (upper row) and perpendicular (lower row) to the crystal c-axis orientation. The isosurface of 60% of the maximum amplitude of wavefunctions is depicted. The color code of the atoms is the same as in Fig. 2. The yellow and cyan lobes correspond to the plus and minus signs of the wavefunction, respectively.

TABLE III. ZFS parameters D and E of $O_CV_{Si}^0$ defects in 4H-SiC calculated using the PBE functional (unit: GHz). The defect structure is optimized using the HSE06 functional. The PAW core contribution is not included in the calculation.

	D	E
$O_CV_{Si\ kk}^0$	1.67	0
$O_CV_{Si\ hh}^0$	1.74	0
$O_CV_{Si\ hk}^0$	1.61	0.15
$O_CV_{Si\ kh}^0$	1.70	0.04

23 October 2026 02:01:49

Published under an exclusive license by AIP Publishing

TABLE IV. Principal values of the hyperfine tensor (A_{xx}, A_{yy}, A_{zz}) of atoms in $O_CV_{Si}^0$ defect in 4H-SiC calculated using the HSE06 functional. The core contribution is included in the calculations. L_O denotes the distance between the atom of interest and the O atom. The hyperfine constants of the O atom, three C atoms with dangling bonds, and nine Si atoms adjacent to those C atoms are shown for the kk, hh, hk, and kh defect complexes. Note that the three C atoms, six out of the nine Si atoms, and three out of the nine Si atoms are equivalent in the kk and hh complexes due to C_{3v} symmetry. By comparison, the number of equivalent C and Si atoms in the hk and kh complexes is reduced due to the symmetry being lowered to C_{1h}.

	Atoms	L_O (Å)	A_{xx} (MHz)	A_{yy} (MHz)	A_{zz} (MHz)
$O_CV_{Si\ kk}^0$	^{17}O	…	5.1	5.1	5.1
	$^{13}C \times 3$	3.43	39.1	38.4	108.0
	$^{29}Si \times 6$	3.75	11.1	10.1	11.8
	$^{29}Si \times 3$	5.00	12.9	12.6	13.5
$O_CV_{Si\ hh}^0$	^{17}O	…	4.9	4.9	5.1
	$^{13}C \times 3$	3.43	46.0	45.3	115.1
	$^{29}Si \times 6$	3.75	10.2	8.9	11.0
	$^{29}Si \times 3$	5.00	12.0	11.8	12.3
$O_CV_{Si\ hk}^0$	^{17}O	…	2.2	2.2	2.5
	^{13}C	3.45	50.1	49.4	109.2
	$^{13}C \times 2$	3.48	39.5	39.0	112.8
	$^{29}Si \times 2$	3.77	8.4	7.2	9.1
	$^{29}Si \times 2$	3.78	11.0	8.8	11.8
	$^{29}Si \times 2$	3.78	11.9	11.0	12.6
	^{29}Si	5.03	10.7	10.6	10.9
	$^{29}Si \times 2$	5.04	13.2	13.1	13.6
$O_CV_{Si\ kh}^0$	^{17}O	…	3.6	3.5	3.7
	$^{13}C \times 2$	3.44	44.6	44.1	114.4
	^{13}C	3.45	47.3	46.3	115.6
	^{29}Si	3.25	11.0	9.3	11.9
	$^{29}Si \times 2$	3.76	10.1	9.1	10.9
	$^{29}Si \times 2$	3.76	10.2	8.9	11.1
	$^{29}Si \times 2$	4.63	11.4	10.6	11.8
	$^{29}Si \times 2$	5.01	12.1	12.0	12.4

the ^{16}O isotope without spin is about 100%, one should be able to observe the hyperfine signals related to oxygens by implantation of ^{17}O ions.

C. Optical properties of the $O_CV_{Si}^0$ defects

Figure 6 is a schematic configuration diagram that illustrates the definitions of the optical parameters investigated in this study; i.e., the absorption and emission energies, ZPL energy, and Stokes and anti-Stokes shifts. Table V summarizes the calculated values of each quantity for the $O_CV_{Si}^0$ defects. For the kk, hh, hk, and kh configurations, we find that the absorption energies are at 1.36, 1.40, 1.25, and 1.34 eV, respectively. Note that these values are quite smaller than the energy differences between the corresponding Kohn–Sham eigenvalues, i.e., 1.75, 1.80, 1.61, and 1.73 eV, respectively, which is due to electron–hole coupling. In either case, however, the order in energy is hh > kk > kh > hk. This implies that although the difference between the eigenvalues overestimates the absolute value of the absorption energy, it is a good measure with

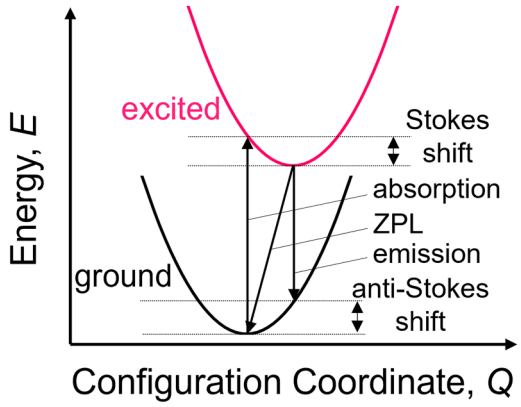


FIG. 6. Schematic configuration diagram illustrating the definitions of the optical parameters listed in Table V; i.e., absorption and emission energies, ZPL energy, and Stokes and anti-Stokes shifts.

which to discuss the energy ordering. The ZPL energies are at 1.19 eV, 1.24 eV, 1.11 eV, and 1.18 eV for the kk, hh, hk, and kh configurations, respectively. Thus, we found that the $O_CV_{Si}^0$ defects have ZPLs in the near-infrared regime (1004–1117 nm), making them attractive candidates for optically active spin qubits.

The squared TDM vector and corresponding radiative lifetime of the ZPL transition were calculated for the $O_CV_{Si}^0$ defect in the kk configuration. As mentioned earlier, we used a 784-atom supercell in order to obtain accurate results. We found that the squared TDM vector is 121 Debye^2, which gives a fairly short radiative lifetime of 12.5 ns. Our calculation also considers the small change in the ZPL energy (1.19 eV → 1.15 eV) due to the change in the supercell size (576-atom → 784-atom). The obtained lifetime is comparable to the calculated values of 11 ns for diamond NV center[54] and 12 ns for V_{Si} in SiC.[18] The μ_z^2 component of the TDM vector is negligibly small (3.76×10^{-7} Debye^2), indicating that the polarization of ZPL is perpendicular to the crystal c-axis, as expected from the symmetry. This situation should also hold for the hh configuration, while hk and kh configurations may have non-negligible contributions from the μ_z^2 component.

Next, we investigated the involvement of phonons in the optical transition. Figure 7 shows the computed PL spectrum of the $O_CV_{Si}^0$ defect in the kk configuration. Here, while the energy of

TABLE V. Optical parameters of $O_CV_{Si}^0$ defects in 4H-SiC obtained using the HSE06 functional with the ΔSCF method (unit: eV). The values are for the lowest energy in-gap transition in the spin minority channel (Fig. 3). $\Delta\varepsilon$ is the energy difference between the Kohn–Sham eigenstates (unit: eV).

	$\Delta\varepsilon$	Absorption	Emission	ZPL	Stokes shift	Anti-Stokes shift
$O_CV_{Si\ kk}^0$	1.75	1.36	1.06	1.19	0.17	0.12
$O_CV_{Si\ hh}^0$	1.80	1.40	1.12	1.24	0.17	0.12
$O_CV_{Si\ hk}^0$	1.61	1.25	0.98	1.11	0.14	0.13
$O_CV_{Si\ kh}^0$	1.73	1.34	1.06	1.18	0.16	0.12

23 October 2026 02:01:49

Published under an exclusive license by AIP Publishing

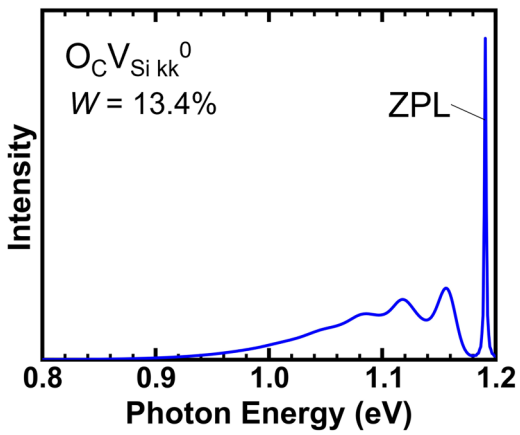


FIG. 7. Calculated PL spectrum of $O_CV_{Si}^0$ defect in the kk configuration in 4H-SiC. The ZPL energy was obtained from the HSE06 functional with the ΔSCF method (Table V). While the HSE06 functional was used to determine the structure of the ground and excited states, the finite displacement method with force constants calculated at a PBE level was used for the phonon calculations. The broadening of ZPL [γ in Eq. (8)] was set to a certain value and is not an output of the calculation. The δ functions in the spectral functions $S(\hbar\omega)$ [Eq. (11)] were replaced by 6-meV-wide Gaussians in order to depict the phonon sidebands.

ZPL was obtained by taking the Jahn-Teller distortion into consideration (Table V), an excited state with restricted C_{3v} symmetry was assumed in the calculation of the phonon side bands. In particular, we set the occupation of each doubly degenerate e state to half as in Refs. 44 and 52. In this way, only fully symmetric phonons should couple to the optical transition. As shown in Fig. 7, phonon side bands appear at lower energies than the ZPL. The calculated total Huang-Rhys factor S is 2.01, corresponding to a high Debye-Waller factor W of 13.4%. It is notable that the Debye-Waller factor of the diamond NV center is only about 3%.[44] The large Debye-Waller factor indicates a large weight of ZPL in the optical spectrum, which is a desirable property for quantum emitters. The large Debye-Waller factor of the $O_CV_{Si}^0$ defect is likely due to the small change in the geometry of the defect upon optical excitation. As a measure of the change in the atomic positions, the ΔQ value calculated for the $O_CV_{Si\,kk}^0$ defect is 0.66 Åamu$^{1/2}$, which is indeed smaller than the reported values for the diamond NV center (0.71 Åamu$^{1/2}$)[44] and the V_1 transition of the SiC V_{Si} defect (0.79 Åamu$^{1/2}$).[52]

D. Discussion

In the earlier stage of SiC research, O-related defect centers were studied using deep-level transient spectroscopy.[55,56] In Ref. 56, O^+ ion implantation was performed in order to vary the mean O concentration over a wide range, 5×10^{14}–1×10^{19} cm^{-3}, and subsequent heat treatment was carried out at temperatures from 1000 °C to 1800 °C. There, O-related shallow donor levels were reported. Soon after, *ab initio* calculations were conducted, which assigned these shallow levels to the double donor O_C defects exhibiting (2+/+) and (+/0) defect levels at $\varepsilon_{VBM}+3.2$ eV and at $\varepsilon_{VBM}+3.1$ eV, respectively.[57] In addition to the above donor levels, Ref. 56 reported O-related deep acceptor levels, i.e., O_{III}, O_{IV}, and O_V. The energy levels of these signals determined from the Arrhenius plot were about $\varepsilon_{VBM}+2.54$ eV, $\varepsilon_{VBM}+2.38$ eV, and $\varepsilon_{VBM}+2.34$ eV. It was speculated that these defects consist either of one or several O atoms or are composed of O atoms and intrinsic defects (vacancies or interstitials). As the calculated (−1/−2) acceptor levels of the O_CV_{Si} defects in this study are in the range of ($\varepsilon_{VBM}+2.40$ eV) – ($\varepsilon_{VBM}+2.52$ eV) (Table II), the observed DLTS signals O_{III} – O_V could be related to the O_CV_{Si} defects. This speculation is further supported by the fact that the formation energy of $O_CV_{Si}^0$ defects is quite low (2.05–2.17 eV: Table I) compared with the calculated values of intrinsic defects in SiC; e.g., V_{Si}: 7.10–7.16 eV, V_C: 4.84–4.88 eV, and C_{Si}: 2.61–2.65 eV in a carbon-rich condition.[38] This indicates a high concentration of O_CV_{Si} defects under a condition close to thermal equilibrium. As we focused on bulk O_CV_{Si} defects and not the surface ones in this study, oxygen ion implantation would be a more reasonable way to create these defects than the thermal oxidation of SiC. By conducting thermal annealing after the implantation, the defects in crystal can dissociate, migrate, or combine with each other and find their stable configurations. Under such a situation, we have a high chance to form the O_CV_{Si} defects because of their low formation energy. We deem that it is now worth revisiting the O-related signals by conducting both PL and DLTS measurements.

Apart from the well-known PL signatures in 4H-SiC due to defects such as V_{Si}[15–17] and $V_{Si}V_C$,[19,20] there are some defect signatures whose origins are still not known. Such signatures include UD_1,[58,59] UD_3,[58,60] and DI_{1-3}.[61] In particular, the ZPL energies of the DI_1, DI_2, and DI_3 defects are 1.236 eV, 1.234 eV, and 1.232 eV, which are close to the ZPL energies, 1.18–1.24 eV, calculated in this study for the $O_CV_{Si}^0$ defects in the hh, kh, and kk configurations (Table V). Furthermore, it was shown that the polarization of the DI_1 and DI_3 signals are perpendicular to the crystal c-axis. This accords with our finding indicating that the ZPL should be polarized perpendicular to the c-axis for the kk and hh configurations due to symmetry arguments. However, in the previous study,[61] the DI defects were speculated to be intrinsic, because they were produced by implantation of different kinds of ions such as Ge, Sn, or Ar with high-temperature annealing at or above 1700 °C. Further studies involving detailed experiments and theoretical considerations are needed in order to support this tentative identification.

IV. SUMMARY

We investigated the OV defect complexes in 4H-SiC by means of *ab initio* calculations. We found that the O_CV_{Si} defects are stable in the neutral charge state with a low formation energy of 2.05–2.17 eV. Furthermore, these defects have a high-spin ground state ($S=1$). Unlike diamond OV centers, where the lowest energy excited state consists of C-O anti-bonding orbitals, the excited state of O_CV_{Si} defects in SiC comprises carbon dangling bond orbitals with a stable optical emission. The ZPL energies of the O_CV_{Si} defects lie in the near-infrared regime, 1.11–1.24 eV (1004–1117 nm). The estimated radiative lifetime of the ZPL transition in the kk configuration is fairly

23 October 2026 02:01:49

Published under an exclusive license by AIP Publishing

short (12.5 ns). Moreover, the estimated Debye-Waller factor is quite high (13.4%) compared with that of diamond NV centers (~3%). We conclude that this defect is an optically active spin defects in SiC that could be used for realizing a spin-to-photon interface.

ACKNOWLEDGMENTS

This work was partly supported by JST, PRESTO Grant No. JPMJPR22B5. This work was achieved through the use of OCTOPUS and SQUID at the Cybermedia Center, Osaka University.

AUTHOR DECLARATIONS

Conflict of Interest

The authors have no conflicts to disclose.

Author Contributions

Takuma Kobayashi: Conceptualization (lead); Data curation (lead); Formal analysis (lead); Funding acquisition (lead); Investigation (lead); Methodology (lead); Project administration (lead); Resources (lead); Validation (lead); Visualization (lead); Writing – original draft (lead); Writing – review & editing (lead). **Takayoshi Shimura:** Investigation (supporting); Writing – review & editing (supporting). **Heiji Watanabe:** Investigation (supporting); Resources (supporting); Writing – review & editing (supporting).

DATA AVAILABILITY

The data that support the findings of this study are available from the corresponding author upon reasonable request.

REFERENCES

[1]J. R. Weber, W. F. Koehl, J. B. Varley, A. Janotti, B. B. Buckley, C. G. Van de Walle, and D. D. Awschalom, Proc. Natl. Acad. Sci. U.S.A. **107**, 8513 (2010).
[2]M. Atatüre, D. Englund, N. Vamivakas, S. Y. Lee, and J. Wrachtrup, Nat. Rev. Mater. **3**, 38 (2018).
[3]D. D. Awschalom, R. Hanson, J. Wrachtrup, and B. B. Zhou, Nat. Photonics **12**, 516 (2018).
[4]A. Gruber, A. Dräbenstedt, C. Tietz, L. Fleury, J. Wrachtrup, and C. V. Borczyskowski, Science **276**, 2012 (1997).
[5]F. Jelezko, T. Gaebel, I. Popa, A. Gruber, and J. Wrachtrup, Phys. Rev. Lett. **92**, 076401 (2004).
[6]D. D. Sukachev, A. Sipahigil, C. T. Nguyen, M. K. Bhaskar, R. E. Evans, F. Jelezko, and M. D. Lukin, Phys. Rev. Lett. **119**, 223602 (2017).
[7]M. K. Bhaskar, D. D. Sukachev, A. Sipahigil, R. E. Evans, M. J. Burek, C. T. Nguyen, L. J. Rogers, P. Siyushev, M. H. Metsch, H. Park, F. Jelezko, M. Lončar, and M. D. Lukin, Phys. Rev. Lett. **118**, 223603 (2017).
[8]G. Thiering and A. Gali, Phys. Rev. B **94**, 125202 (2016).
[9]N. Ghafari Cherati, G. Thiering, and Á Gali, J. Phys.: Condens. Matter **35**, 315502 (2023).
[10]T. Kimoto and J. A. Cooper, *Fundamentals of Silicon Carbide Technology* (John Wiley & Sons, Singapore, 2014).
[11]N. T. Son, C. P. Anderson, A. Bourassa, K. C. Miao, C. Babin, M. Widmann, M. Niethammer, J. Ul Hassan, N. Morioka, I. G. Ivanov, F. Kaiser, J. Wrachtrup, and D. D. Awschalom, Appl. Phys. Lett. **116**, 190501 (2020).
[12]S. Castelletto and A. Boretti, J. Phys. Photonics **2**, 022001 (2020).
[13]L. P. Yang, C. Burk, M. Widmann, S. Y. Lee, J. Wrachtrup, and N. Zhao, Phys. Rev. B **90**, 241203(R) (2014).
[14]H. Seo, A. L. Falk, P. V. Klimov, K. C. Miao, G. Galli, and D. D. Awschalom, Nat. Commun. **7**, 12935 (2016).
[15]E. Janzén, A. Gali, P. Carlsson, A. Gällström, B. Magnusson, and N. T. Son, Mater. Sci. Forum **615–617**, 347 (2009).
[16]M. Widmann, S. Y. Lee, T. Rendler, N. T. Son, H. Fedder, S. Paik, L. P. Yang, N. Zhao, S. Yang, I. Booker, A. Denisenko, M. Jamali, S. A. Momenzadeh, I. Gerhardt, T. Ohshima, A. Gali, E. Janzén, and J. Wrachtrup, Nat. Mater. **14**, 164 (2015).
[17]P. G. Baranov, A. P. Bundakova, A. A. Soltamova, S. B. Orlinskii, I. V. Borovykh, R. Zondervan, R. Verberk, and J. Schmidt, Phys. Rev. B **83**, 125203 (2011).
[18]P. Udvarhelyi, R. Nagy, F. Kaiser, S. Y. Lee, J. Wrachtrup, and A. Gali, Phys. Rev. Appl. **11**, 044022 (2019).
[19]W. F. Koehl, B. B. Buckley, F. J. Heremans, G. Calusine, and D. D. Awschalom, Nature **479**, 84 (2011).
[20]B. Magnusson, N. T. Son, A. Csóré, A. Gällström, T. Ohshima, A. Gali, and I. G. Ivanov, Phys. Rev. B **98**, 195202 (2018).
[21]K. C. Miao, A. Bourassa, C. P. Anderson, S. J. Whiteley, A. L. Crook, S. L. Bayliss, G. Wolfowicz, G. Thiering, P. Udvarhelyi, V. Ivády, H. Abe, T. Ohshima, Á. Gali, and D. D. Awschalom, Sci. Adv. **5**, eaay0527 (2019).
[22]Y. Hijikata, T. Horii, Y. Furukawa, Y. I. Matsushita, and T. Ohshima, J. Phys. Commun. **2**, 111003 (2018).
[23]Y. Matsushita, Y. Furukawa, Y. Hijikata, and T. Ohshima, Appl. Surf. Sci. **464**, 451 (2019).
[24]P. Hohenberg and W. Kohn, Phys. Rev. **136**, B864 (1964).
[25]W. Kohn and L. J. Sham, Phys. Rev. **140**, A1133 (1965).
[26]P. E. Blöchl, Phys. Rev. B **50**, 17953 (1994).
[27]G. Kresse and J. Furthmüller, Phys. Rev. B **54**, 11169 (1996).
[28]G. Kresse and D. Joubert, Phys. Rev. B **59**, 1758 (1999).
[29]J. Heyd, G. E. Scuseria, and M. Ernzerhof, J. Chem. Phys. **118**, 8207 (2003).
[30]J. Heyd, G. E. Scuseria, and M. Ernzerhof, J. Chem. Phys. **124**, 219906 (2006).
[31]J. P. Perdew, K. Burke, and M. Ernzerhof, Phys. Rev. Lett. **77**, 3865 (1996).
[32]V. Wang, N. Xu, J. C. Liu, G. Tang, and W. T. Geng, Comput. Phys. Commun. **267**, 108033 (2021).
[33]K. Momma and F. Izumi, J. Appl. Crystallogr. **44**, 1272 (2011).
[34]M. Leslie and M. J. Gillan, J. Phys. C: Solid State Phys. **18**, 973 (1985).
[35]J. P. Perdew, R. G. Parr, M. Levy, and J. L. Balduz, Phys. Rev. Lett. **49**, 1691 (1982).
[36]S. Lany and A. Zunger, Phys. Rev. B **80**, 085202 (2009).
[37]P. Deák, B. Aradi, T. Frauenheim, E. Janzén, and A. Gali, Phys. Rev. B **81**, 153203 (2010).
[38]T. Kobayashi, K. Harada, Y. Kumagai, F. Oba, and Y. I. Matsushita, J. Appl. Phys. **125**, 125701 (2019).
[39]V. Ivády, T. Simon, J. R. Maze, I. A. Abrikosov, and A. Gali, Phys. Rev. B **90**, 235205 (2014).
[40]K. Szász, T. Hornos, M. Marsman, and A. Gali, Phys. Rev. B **88**, 075202 (2013).
[41]V. Ivády, I. A. Abrikosov, and A. Gali, Npj Comput. Mater. **4**, 76 (2018).
[42]O. V. Yazyev, I. Tavernelli, L. Helm, and U. Röthlisberger, Phys. Rev. B **71**, 115110 (2005).
[43]A. Gali, E. Janzén, P. Deák, G. Kresse, and E. Kaxiras, Phys. Rev. Lett. **103**, 186404 (2009).
[44]A. Alkauskas, B. B. Buckley, D. D. Awschalom, and C. G. Van De Walle, New J. Phys. **16**, 073026 (2014).
[45]V. Ivády, J. Davidsson, N. T. Son, T. Ohshima, I. A. Abrikosov, and A. Gali, Phys. Rev. B **96**, 161114(R) (2017).
[46]J. Davidsson, V. Ivády, R. Armiento, N. T. Son, A. Gali, and I. A. Abrikosov, New J. Phys. **20**, 023035 (2018).
[47]Q. Zheng, see https://Github.Com/Liming-Liu/Pyvaspwfc for "PyVaspwfc" (2018).
[48]J. Davidsson, J. Phys.: Condens. Matter **32**, 385502 (2020).
[49]R. Kubo and Y. Toyozawa, Prog. Theor. Phys. **13**, 160 (1955).
[50]A. Togo and I. Tanaka, Scr. Mater. **108**, 1 (2015).
[51]S. A. Tawfik and S. P. Russo, Comput. Phys. Commun. **273**, 108222 (2022).
[52]A. Hashemi, C. Linderälv, A. V. Krasheninnikov, T. Ala-Nissila, P. Erhart, and H. P. Komsa, Phys. Rev. B **103**, 125203 (2021).

23 October 2026 02:01:49

Published under an exclusive license by AIP Publishing

[53]A. Gali, M. Fyta, and E. Kaxiras, Phys. Rev. B **77**, 155206 (2008).
[54]P. Siyushev, H. Pinto, M. Vörös, A. Gali, F. Jelezko, and J. Wrachtrup, Phys. Rev. Lett. **110**, 167402 (2013).
[55]O. Klettke, G. Pensl, T. Kimoto, and H. Matsunami, Mater. Sci. Forum **353–356**, 459 (2001).
[56]T. Dalibor, H. Trageser, G. Pensl, T. Kimoto, H. Matsunami, D. Nizhner, O. Shigiltchoff, and W. J. Choyke, Mater. Sci. Eng. B **61–62**, 454 (1999).
[57]A. Gali, D. Heringer, P. Deák, Z. Hajnal, T. Frauenheim, R. P. Devaty, and W. J. Choyke, Phys. Rev. B **66**, 125208 (2002).
[58]B. Magnusson and E. Janzén, Mater. Sci. Forum **483–485**, 341 (2005).
[59]E. N. Kalabukhova, D. V. Savchenko, S. Greulich-Weber, M. F. Bulanyi, S. A. Omelchenko, O. V. Khmelenko, A. A. Gorban, and E. N. Mokhov, Mater. Sci. Forum **527–529**, 651 (2006).
[60]M. Wagner, B. Magnusson, W. M. Chen, and E. Janzén, Phys. Rev. B **66**, 115204 (2002).
[61]T. Kobayashi, M. Rühl, J. Lehmeyer, L. K. S. Zimmermann, M. Krieger, and H. B. Weber, J. Phys. D: Appl. Phys. **55**, 105303 (2022).

23 October 2026 02:01:49

Published under an exclusive license by AIP Publishing